

Local Dielectric Measurements of BaTiO₃-CoFe₂O₄ Nano-composites Through Microwave Microscopy

Yi Qi and Steven M. Anlage

*Materials Research Science and Engineering Center, Departments of Physics and Materials Science and Engineering,
University of Maryland, College Park*

H. Zheng and R. Ramesh

Department of Materials Science and Engineering, University of California at Berkeley

We report on linear and non-linear dielectric properties measurements of BaTiO₃ – CoFe₂O₄ (BTO-CFO) ferroelectro-magnetic nano-composites and pure BaTiO₃ and CoFe₂O₄ samples with Scanning Near Field Microwave Microscopy. The permittivity scanning image with spatial resolution of 1 μm shows the nano-composites have very uniform quality with effective dielectric constant $\epsilon_r = 140 \pm 6.4$ at 3.8 GHz and room temperature. The temperature dependence of dielectric permittivity shows the Curie temperature of pure BTO was shifted by the clamping effect from the MgO substrate, whereas the Curie temperature shift of the BTO ferroelectric phase in BTO-CFO composites arises mainly from the CFO. Non-linear dielectric measurements of BTO-CFO show good ferroelectric properties from the BTO. This experiment also provides for the possibility of localized measurement of the Magneto-Electric effect using microwave microscopy upon applying a strong magnetic field.

Introduction

Ferroelectro-magnets are materials in which magnetic and electric dipolar orderings coexist. Because of the additional degree of freedom, there is current interest in using the materials for applications such as memory, electric field-controlled ferromagnetic resonance device, magnetically switched electro-optical device, etc. [1].

Besides single phase ferroelectro-magnetic materials [2-3], researchers have developed multiphase materials consisting of layers or mixtures of piezoelectric and magnetostrictive phases [4-5]. The prospective coexistence in these multiphase materials of both ferroelectric and ferromagnetic orders makes them attractive for magneto-electric coupling studies. Some coupling investigations have been made through the magnetically tunable dielectric properties measurements [6-7] or the dielectric anomalies at the magnetic transition temperature [8-9]. Thus the dielectric measurements become fundamentally important especially if we can improve the sensitivity or make the measurement localized to find the nanostructure/composition dependence of properties. In this paper, we introduce localized dielectric measurements of BTO-CFO using a microwave microscope. We report the measurement of relative dielectric constant with good sensitivity (about 4 in the range of 200~1000) and with high spatial resolution (~1 μm). Another motivation of this paper is to investigate the change in ferroelectric properties of the BTO due to the introduction of the secondary phase CFO. We measured the temperature dependence and electric field tunability of the dielectric properties on these new materials and compared with a pure BTO thin film. The results show evidence that the BTO dielectric properties are significantly affected by the CFO pillars.

Experiments

Our scanning microwave microscope consists of an open-ended coaxial probe with a sharp, protruding center conductor [10]. The sample under the tip perturbs the resonator and causes a frequency shift. The frequency shift from the unperturbed condition (with a known sample as reference) to the perturbed condition (with the unknown sample to be measured) is related to the permittivity of the sample. Using perturbation theory [11], we calculated the frequency shift of the microscope as a function of the fields in the sample near the probe tip, [10]

$$\frac{\Delta f}{f} \approx \frac{\epsilon_0}{4W} \int_{V_s} (\epsilon_{r2} - \epsilon_{r1}) \vec{E}_1 \cdot \vec{E}_2 dV,$$

where ϵ_{r2} and ϵ_{r1} are the relative permittivity of the two samples. E_1 and E_2 are the calculated electric fields inside the two samples, W is the energy stored in the resonator, and the integral is over the volume V_s of the sample.

The dielectric constant vs. frequency shift curve for bulk and thin film samples are illustrated in Fig 1. The shape of curve is determined by the probe geometry. Here we simplify the probe geometry as an ellipsoid of revolution with a blunt end (illustrated in Fig2. (c)). The geometry can be modified by varying three parameters, i.e. long axis a , short axis b and blunt end width c . For a defined geometry, we use Maxwell 2D software (Ansoft) to calculate the static electric field and stored energy in

the sample. It is established that the static fields are a good approximation to the near-field structure of the tip.^[10] Combined with the equation above, the frequency shift vs. permittivity curve is calculated. To find the probe geometry of the tip used in our experiment, i.e. the correct a , b , and c parameters, calibration points were measured with several known samples. Fig 1.(a) shows a simulated curve of frequency shift vs. permittivity that fits our calibration points well when we choose $a=50\mu\text{m}$, $b=22\mu\text{m}$ and $c=2.6\mu\text{m}$. The geometry parameters are confirmed by SEM observation of the tip^[12]. We can see that larger dielectric permittivity causes more negative frequency shift of the microscope.

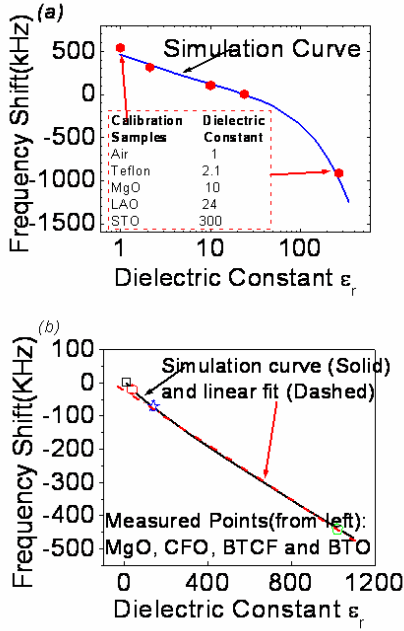


Fig 1. (a) Simulation curve of frequency shift vs. permittivity for bulk samples (we use a bulk LAO substrate as the reference and all frequency shifts are given relative to it), and (b) for thin films. We assume MgO as substrate and the thin film thickness is 180nm. All frequency shifts are given relative to MgO

Fig 1.(b) simulates the thin film situation with the probe geometry determined by step (a). In this simulation, we assume the substrate is MgO and the thin film thickness is 180nm, which is consistent with the samples used in this experiment. In Fig 1.b we define the bare MgO substrate as the unperturbed condition, the frequency shift relative to MgO is recorded to get the dielectric permittivity for the thin film samples to be measured. The simulation curve is close to a straight line in the range from $\epsilon_r=100$ to $\epsilon_r=1100$ ($\epsilon_r \approx -15.425 - 2.336 \Delta f$ (kHz)), so we can use the linear fit to estimate the dielectric constant of the thin films.

The BTO-CFO thin film nano-composite material is prepared by

pulsed-laser deposition on MgO substrates. All films discussed here have a nominal thickness of 180nm. X-ray diffraction and TEM experiments show that the BTO and CFO were separated into two phases in the thin film by self-assembly^[13]. The two phases have a pillar-in-matrix geometry, in which the CFO pillars occupy about 35% in volume and have diameters of 20-30 nm, and their distribution and size are roughly uniform. Both BTO and CFO phases have their [100] lattice direction perpendicular to the thin film plane^[13].

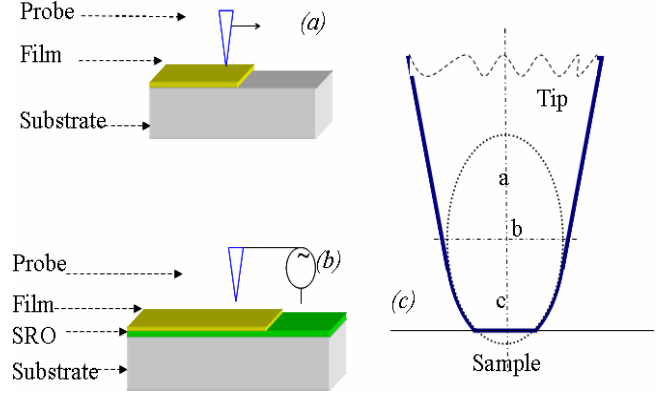


Fig 2. (a) Sample schematic for dielectric measurements (BTO-CFO, pure BTO or pure CFO thin film directly on MgO substrate with partly exposed MgO) (b) Sample schematic for non-linear dielectric measurements (BTO-CFO, pure BTO or pure CFO thin film on MgO substrate with a SRO counter-electrode layer) (c) Simplified geometry of the probe tip as an ellipsoid of revolution.

Two types of BTO-CFO samples were prepared. One without a counter-electrode for linear dielectric measurement (a) and another one with a counter-electrode SrRuO₃ (SRO) layer for non-linear dielectric measurement (b). The sheet resistance of the SRO layer is 2700 Ω /square, sufficiently large to render it effectively invisible to the microwave signal to good approximation. For the former samples, part of the thin film was ion milled to expose the MgO substrate (see Fig 2.a). Again, we use the MgO substrate as the unperturbed condition and the BTO-CFO on MgO as the perturbed condition while measuring the frequency shift. For the latter case, we use a bias tee outside the inductively de-coupled resonator to apply bias voltage between the SRO counter-electrode and the microscope tip to get the dielectric vs. bias voltage relationship (Fig 2.b)^[10]. For comparison purposes, pure BTO and pure CFO thin film samples were also prepared with the same geometry and lattice direction, that is BTO on MgO (c) and BTO on SRO counterelectrode on MgO substrate(d), CFO on MgO (e) and CFO on SRO counterelectrode on MgO substrate(f).

Results and Discussions

We scanned the microwave microscope tip across the edge between the BTO-CFO thin film and MgO bare substrate and recorded the frequency shift. We use this design rather than measuring two separate samples because it can reduce the systematic error and noise, especially for the temperature dependence measurements presented below. There is a sharp change in frequency shift upon crossing the edge from MgO to BTO-CFO or BTO (Fig 3). The negative frequency change from MgO to BTO-CFO or BTO indicates BTO-CFO and BTO have higher permittivity than MgO ($\epsilon_r \sim 10$). We can convert the frequency shift values to relative permittivity values of $\epsilon_r = 140 \pm 6$, 1020 ± 20 and 35 ± 2 for BTO-CFO, BTO and CFO respectively (at room temperature and 3.8 GHz). Assuming that the patterned edge and dielectric properties have a sharp change at the edge, from the scan with $0.1 \mu\text{m}$ step size (inset of Fig 3. (b)), we can also see the microwave microscope has a quantitative resolution for dielectric constant of about $5 \mu\text{m}$ [14].

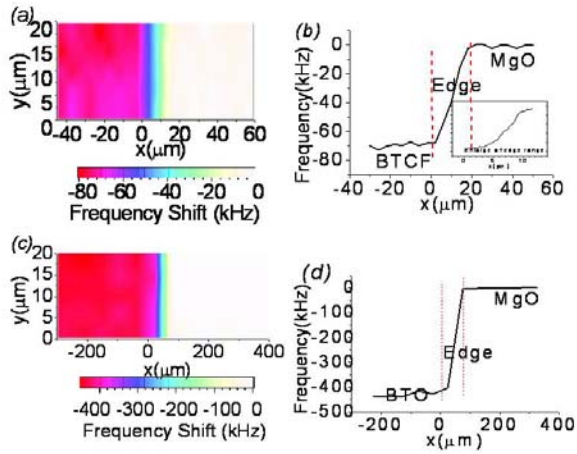


Fig 3. (a) (c) Frequency shift scanning image at 3.8 GHz and room temperature crossing BTO-CFO/MgO edge and BTO/MgO edge respectively, (b) (d) Single line scans corresponding to (a) and (c), inset of (b) is a scan across the BTO-CFO/MgO edge with $0.1 \mu\text{m}$ step size.

Another scanning image [Fig 4. (a)] shows that the BTO-CFO has a fairly uniform dielectric property $\epsilon_r = 140 \pm 6.4$ averaged over a $2\text{mm} \times 2\text{mm}$ area. The dielectric properties of this kind of nano-composite mainly depend on composition [5]. From TEM and AFM measurement of this sample [13], we see it has roughly the same composition in the plane of the film. That may explain the small range of dielectric constant variation observed. Fig 4. b shows a finer scanning image with $0.5 \mu\text{m}$ step size. The dielectric constant is $\epsilon_r = 136 \pm 8.2$ over this area. There is still contrast in the dielectric image on this short length scale. It is also clear that the smallest feature resolved (i.e. the qualitative resolution [14]) is a single pixel, or $0.5 \mu\text{m}$. However, the

resolution for quantitative imaging is larger and is typically governed by the tip geometry.

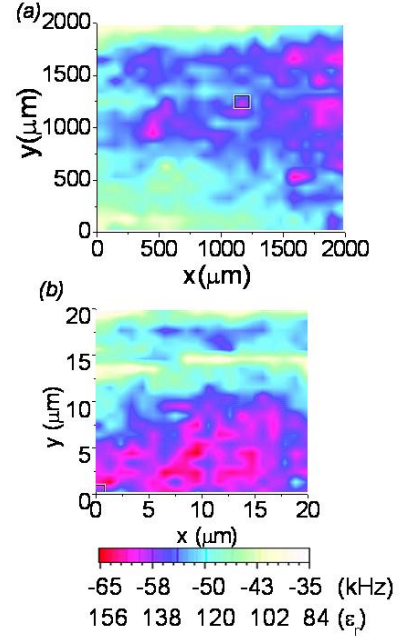


Fig 4. (a) Dielectric image of BTO-CFO, $2000 \mu\text{m} \times 2000 \mu\text{m}$ scanning area with $5 \mu\text{m}$ step size, and (b) $20 \mu\text{m} \times 20 \mu\text{m}$ area scanning image with $0.5 \mu\text{m}$ step size, both taken at 3.8 GHz and room temperature.

The frequency shifts across the edge from MgO to BTO-CFO or BTO were recorded as a function of sample temperature from $30^\circ\text{C} \sim 200^\circ\text{C}$. Fig 5 show the temperature dependence of the frequency shift, which can be converted to temperature dependence of dielectric permittivity (we used the linear fit of $\epsilon_r \sim \Delta f$ curve shown in Fig.1 b). Due to the lattice transition of the perovskite structure of the BTO crystal, the relative dielectric permittivity should have a peak at the Curie temperature [15]. Firstly, we used a BTO bulk single crystal to verify this trend and to calibrate the thermometer from the transition temperature. Fig. 5(a) inset shows the dielectric change of the BTO crystal with temperature. There is a peak at 120°C , which is consistent with the Curie temperature from the literature [16]. The room temperature frequency shift corresponds to a permittivity of $\epsilon_r \sim 800$ (using the simulation curve for bulk samples in Fig. 1(a)), which is on the same order as the results for the thin film BTO sample.

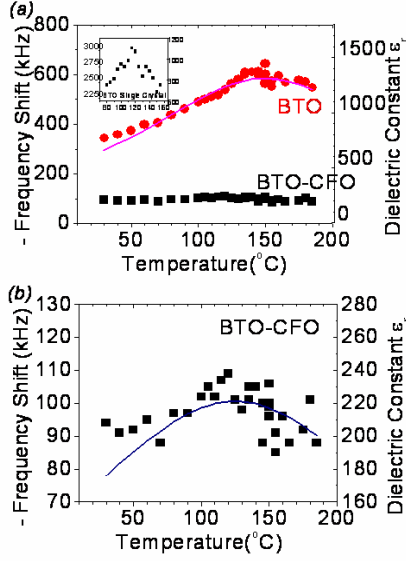


Fig 5. (a) Temperature dependence of dielectric constant for BTO thin film (red points), BTO-CFO thin film (black points), and bulk BTO single crystal (inset); (b) enlargement of BTO-CFO curve in (a). Also shown as solid lines on BTO and BTO-CFO are fits to the generalized Curie-Weiss equation discussed in the text. All data taken at 3.8 GHz.

BTO and BTO-CFO thin films on MgO also show a peak in $\epsilon_r(T)$ which corresponds to the lattice transition of the BTO phase. However the broadening and flattening of the peak is typical of diffuse transitions, which can be attributed to structural inhomogeneity resulting from reduced grain size^[15] and the strain gradient induced by the epitaxial growth of the thin films^[17]. The broadened peak can be fit using a generalized Curie-Weiss equation^[18]:

$$\frac{1}{\epsilon} = \frac{1}{\epsilon_{\max}} + \frac{(T - T_{\max})^2}{2\epsilon_{\max}\delta^2},$$

where the transition temperature is defined by T_{\max} , which corresponds to the maximum dielectric constant ϵ_{\max} , and δ is the diffuseness coefficient.

Large values of the coefficient δ indicate a strongly diffuse transition. Here we found $\delta = 94$ and 129 , and transition temperatures $T_{\max} = 154^\circ\text{C}$ and 124°C for BTO and BTO-CFO thin films, respectively. The transition temperature shifts are due to the stress from the substrate or the CFO phase^[15, 19]. There is a lattice mismatch between BTO and CFO and this mismatch causes stress on the BTO phase and further causes a dielectric and Curie temperature change. The CFO thin film on MgO does not show an

obvious temperature dependence in $\epsilon_r(T)$ (not shown here).

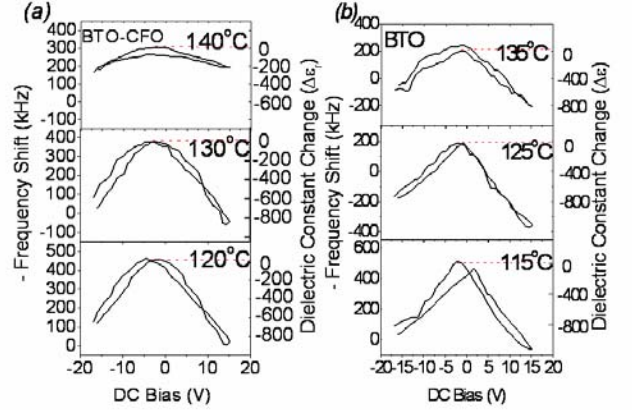


Figure 6. Local dielectric tunability measurements at 3.8 GHz and room temperature on (a) BTO-CFO and (b) BTO films performed at different temperatures. The right axis shows the dielectric constant change relative to zero DC bias voltage, 100 kHz of frequency shift corresponds to about $\Delta\epsilon_r \sim 200$.

The dielectric tunability measurements were done at a single point on similar thin films but with an SRO counterelectrode present (Fig 2.b). The results show that BTO-CFO has a non-linear dielectric property similar in magnitude to BTO (Fig. 6). Applying a bias voltage, the dielectric permittivity is reduced, so that with 0 bias voltage the dielectric has a maximum value. Further measurement on CFO/SRO as a function of bias voltage shows only frequency shift change at the noise level of the experiment. Hence we conclude that the non-linearity in BTO-CFO/SRO comes from the BTO phase and not the SRO layer. The peak in the tunability curve corresponds to the reversal of polarization (coercive field), and the amplitude of $\Delta\epsilon_r$ corresponds to the amount of switchable polarization^[20]. Therefore, with decreasing temperature below T_c , the tunability curve will exhibit a higher permittivity peak and a more pronounced hysteresis in which the upgoing and downgoing frequency shift curves cross. Above T_c , the BTO is in the paraelectric state, the tunability curves exhibit a weak hysteresis behavior.^[21] In our experiment, this transition occurs at 130°C (for BTO-CFO) or 125°C (for BTO) (see Fig. 6).

For BTO-CFO films the transition temperature determined from the dielectric measurement is the same as that from non-linear measurement, with or without the counter-electrode. It appears that the Curie temperature shift of BTO-CFO is mainly caused by the CFO phase, either

through stress caused by lattice mismatch or Co and Fe diffusing into the BTO phase leading to a metastable solid solution^[5]. For pure BTO, the transition temperature determined from linear dielectric measurements is different from that by non-linearity measurements. We believe the shift of the BTO Curie temperature is caused by the substrate clamping effect. Introducing an SRO counter-electrode layer would change the stress thus changing the Curie temperature of the film.

Summary

In summary, we measured the linear and non-linear dielectric properties of BTO-CFO nano-composites. The dielectric properties of BTO-CFO are similar to those of BTO including the temperature dependence and bias voltage dependence. The measurement has a qualitative spatial resolution as high as 0.5 μm . The dielectric change as well as the transition temperature change in the BTO component of BTO-CFO is mainly due to the interaction of BTO with CFO.

With this localized dielectric measurement technique, we also have the possibility of measuring the magneto-electric effect locally. Because applying a magnetic field would induce a magnetostriction of the CFO phase, this strain is transferred to BTO, which is equivalent to the stress effect on BTO. Our microscope has a sensitivity of 2 kHz in frequency shift, which corresponds to $\Delta\epsilon_r \sim 4$ in the 200-1000 relative dielectric constant range. Based on piezoelectric and magnetostriction coefficients ($e_{33} = 18.6 \text{ C/m}^2$, $q_{33} = 699.7 \text{ N/Am}$)^[22], we estimate that a magnetic field of 3000 Oersted is needed to get a measurable dielectric change in the BTO-CFO film. The advantage for the proposed magneto-electric measurement is that we can localize it to the μm scale. This provides us the capability to investigate the relation between magneto-electric properties and local composition or nano-structure. Further experiments are underway in which we apply a strong magnetic field and reduce the noise level of the microscope.

Acknowledgements:

We gratefully acknowledge assistance from Alexander Tselev and Atif Imtiaz. This work was supported by the MRSEC under contract DMR-00-80008 and DMR-05-20471.

1. Van E. Wood and A. E Austin, Possible applications for magnetoelectric materials, *Int. J. Magnetism*, **5**, 303-315 (1974).
2. G. A. Smolenskii and I. E. Chupis, Ferroelectromagnets, *Sov. Phys. Usp.* **25**, 475 (1982).

3. B. I. Al'shin and D.N. Astrov, Magnetolectric effect in Titanium Oxide Ti_2O_3 , *Soviet Physics JETP*, **17**,4, 809 (1963).
4. J. G. Wan and J. M. Liu *et. al.* Giant magnetoelectric effect of a hybrid of magnetostrictive and piezoelectric composites. *J. Appl. Phys.* **93**, 9916 (2003).
5. K.-S. Chang *et. al.* , Exploration of Artificial Multiferroic Thin Film Heterostructures Using Composition Spreads, *Appl. Phys. Lett.*, **84**, 3091 (2004).
6. Kimura, T. *et al.* Magnetocapacitance effect in multiferroic BiMnO_3 . *Phys. Rev. B*, **67**, 180401 (2003).
7. Baturov, L. N., Al'shin, B. I. & Yarmukhamedov, Yu. N. Nonlinear magnetoelectric and dielectric properties of Ni-I boracite. *Fiz. Tverd. Tela* **20**, 2254–2259 (1978); *Sov. Phys. Solid State*, **20**, 1300–1303 (1978).
8. Scott, J. F. Phase transitions in BaMnF_4 . *Rep. Prog. Phys.* **12**, 1056–1084 (1979).
9. Katsufuji, T. *et al.* Dielectric and magnetic anomalies and spin frustration in hexagonal RMnO_3 . *Phys. Rev. B*, **64**, 104419 (2001).
10. D. E. Steinhauer, C.P. Vlahacos, F.C. Wellwood, and S. M. Anlage, Quantitative imaging of dielectric permittivity and tunability with a near field scanning microwave microscope, *Rev. Sci. Instrum.* **71**, 2751 (2000).
11. H. M. Altshuler, in *Handbook of Microwave Measurements II*, edited by M. Sucher and J. Fox (Polytechnic Inst. Of Brooklyn, Brooklyn, NY 1962) p. 225.
12. Atif Imtiaz , Marc Pollak , Steven M. Anlage, John D. Barry and John Melngailis , Near-field microwave microscopy on nanometer length scales, *J. Appl. Phys.* **97**, 044302 (2005).
13. H. Zheng, J.Wang, R.Ramesh *et al.*, Multiferroic $\text{BaTiO}_3\text{-CoFe}_2\text{O}_4$ nanostructures, *Science*, **303**, 661 (2004).
14. Steven M. Anlage, Vladimir V. Talanov, and Andrew R. Schwartz, Principles of Near-Field Microwave Microscopy, section 4.7, *Scanning Probe Microscopy: Electrical and Electromechanical Phenomena at the Nanoscale*, edited by S. Kalinin and A. Gruverman (Springer, New York, 2006).
15. B. H. Hoerman, G. M. Ford, L.D. Kaufmann, and B.W. Wessels, Dielectric properties of epitaxial BaTiO_3 thin films, *Appl. Phys. Lett.*, **73**, 16 (1998).
16. Sakayori K, Matsui Y, Abe H, *et al.* Japanese Journal of Applied Physics Part 1 – Regular papers short notes & review papers, **34**(9B), 5443-5445 (1995).
17. Sinnamon, L. J., Bowman, R. M. & Gregg, J. M. Thickness-induced

stabilization of ferroelectricity in SrRuO₃/Ba_{0.5}Sr_{0.5}TiO₃/Au thin film capacitors. Appl. Phys. Lett., **81**, 889-891 (2002).

18. C. B. Parker, J.-P. Maria, and A. I. Kingon, Temperature and thickness dependent permittivity of (Ba,Sr)TiO₃ thin films, Appl. Phys. Lett., **81**, 340 (2002).
19. V. Moshnyaga *et. al*, Structural phase transition at the percolation threshold in epitaxial (La_{0.7}Ca_{0.3}MnO₃)_{1-x}:(MgO)_x nanocomposite films, Nature Materials **2**, 247 (2003).
20. S. L. Miller, R. D. Nasby, J. R. Schwank, M. S. Rodgers, and P. V. Dressendorfer, Device modeling of ferroelectric capacitors, J. Appl. Phys. **68**, 6463 (1990).
21. J Miao, B R Zhao *et. al*. Temperature dependence of the ferroelectric and dielectric properties of the BST/LSMO heterostructure, J. Phys. D: Appl. Phys. **38**, 5 (2005).
22. Ce-Wen Nan, Magneto-electric effect in composites of piezoelectric and piezomagnetic phases, Phys. Rev. B **50**, 9, 6082 (1994).

